GIS Analysis of Global Impacts from Sea Level Rise

Xingong Li, Rex J. Rowley, John C. Kostelnick, David Braaten, Joshua Meisel, and Kalonie Hulbutta

Abstract

Future sea level rise caused by climate change would disrupt the physical processes, economic activities, and social systems in coastal regions. Based on a hypothetical global sea level increase of one to six meters, we developed GIS methods to assess and visualize the global impacts of potential inundation using the best available global datasets. After susceptible areas were delineated, we estimated that the size of the areas is between 1.055 (one meter) to 2.193 million km^2 (six meters). Population in the susceptible areas was estimated to range from 108 (one meter) to 431 million (six meters) people. Among the seven land-cover types in the susceptible areas, forest and grassland account for more than 60 percent for all the increments of sea level rise. A suite of interactive visualization products was also developed to understand and communicate the ramifications of potential sea level rise.

Introduction

During the twentieth century, sea level has risen about 0.17 $\pm$ 0.05 meters (IPCC, 2007). Without including the increased glacial output to the sea, the Intergovernmental Panel on Climate Change (IPCC) also estimated that the rate of sea level rise will roughly double during the next century due to increasing global temperature, with an upper range of sea level rise of 0.59 m by 2100. Church and White (2006) discovered a significant acceleration of sea level rise in the twentieth century and estimated a sea level rise from 2.0 to 3.4 meters between 1990 and 2100 if the acceleration remains constant. Nearly a quarter of the world's population lives at elevations below 100 m from mean sea level and within 100 km from a coast (Nicholls and Small, 2002). Furthermore, coastal regions have the greatest concentration of economic activities (Nicholls and Tol, 2006). Flooding caused by sea level rise will likely disrupt the physical processes, economic activities, and social systems in the coastal regions. To assist policy makers as well as the general public in understanding the risks, a global analysis of the impacts posed by sea level rise is needed even though the impacts in specific regions are better known (Marbaix and Nicholls, 2007).

Numerous assessments of present and future coastal impacts of sea level rise have been conducted at regional and local scales. Several studies have been conducted for the United States by individual researchers (Zhang *et al.*, 2004; Boruff *et al.*, 2005), the United States Geological Survey (USGS) (Thieler *et al.*, 2000), and the U.S. Environmental Protection Agency (EPA) (Titus *et al.*, 1991). Huang *et al.* (2004) examined the potential risk of tidal inundation due to future sea level rise in the Pearl River delta, China, and found that a large part of the delta plain will be vulnerable to tidal inundation with a sea level rise as small as 30 cm. Cooper *et al.* (2005) examined the potential impacts of sea level rise on the New Jersey coast and proposed a range of adaptation and mitigation possibilities. At a local scale, Wu *et al.* (2002) showed that sea level rise will increase considerably the vulnerability of Cape May County, New Jersey, to flood hazards by increasing the areas that are exposed to the highest flood risk. Hennecke *et al.* (2004) applied a GIS and two coastal behavior models to estimate the vulnerability of a 10 km segment of beach to sea level rise and/or coastal storms.

Only a few researchers have studied the *global* impacts of sea level rise using GIS analysis and global datasets that are now readily available. Nicholls *et al.* (1999), Nicholls (2002 and 2004), and Nicholls and Tol (2006) examined the potential impacts of global sea level rise on coastal flooding. Their analyses are at the scale of coastal countries and are limited by the assumptions that the coastal country polygons have a constant slope and that the population distribution within the polygons is uniform. Weiss and Overpeck (2003) mapped susceptible areas globally but did not extend their analysis to examine the impacts of sea level rise on land-cover and population. Dasgupta *et al.* (2007) reported the impacts of sea level rises on 84 developing counties. The population data

Xingong Li and David Braaten are at the University of Kansas, Department of Geography, 1475 Jayhawk Blvd., Lawrence, KS 66045 and the Center for Remote Sensing of Ice Sheets (CReSIS) (lixi@ku.edu).

Rex J. Rowley is at Haskell Indian Nations University, College of Arts and Science, 155 Indian Avenue, Lawrence, KS 66046.

John C. Kostelnick is at Illinois State University, Department of Geography-Geology, Campus Box 4400, Normal, IL 61790, and formerly at Haskell Indian Nations University, College of Arts and Science, Lawrence, KS 66046.

Joshua Meisel is at the Center for Remote Sensing of Ice Sheets (CReSIS), and formerly at Haskell Indian Nations University, College of Arts and Science, Lawrence, KS 66046.

Kalonie Hulbutta is at the United States Census Bureau, and formerly at Haskell Indian Nations University, College of Arts and Science, 155 Indian Avenue, Lawrence, KS 66046, and the Center for Remote Sensing of Ice Sheets (CReSIS).

Photogrammetric Engineering & Remote Sensing
Vol. 75, No. 7, July 2009, pp. 807–818.

0099-1112/09/7507–0807/$3.00/0

used in their analysis, however, is limited by its spatial resolution at the country level, and the digital elevation model (DEM) they used does not cover the entire globe. In addition, their GIS methods relied on manual editing of simply delineated potential inundation zones.

As a tool for managing and analyzing geographic data, GIS has been used to delineate potentially inundated areas (hereafter PIAs) resulting from projected sea level rises (Gornitz *et al.*, 2001; Titus and Richman, 2001; Cooper *et al.*, 2005; Dasgupta *et al.*, 2007). In most of those analyses, PIAs were identified if their elevation is below a projected sea level rise. Although the method is simple, it has two shortcomings. First, water connectivity is not considered when PIAs are delineated. Some areas, even though their elevation is below a projected sea level rise, should not be considered PIAs if terrain barriers exist between the ocean and the areas. Second, some of the areas with an elevation below the projected sea level rise already exist as inland water bodies, and therefore should not be included in the PIAs[1]. Due to these two shortcomings, such simple GIS methods will overpredict PIAs. In addition, when the analysis is performed at a global scale within a GIS, calculating the size of PIAs is plagued by the fact that the cells on a global raster layer are quadrilateral regions with changing sizes. Dasgupta *et al.* (2007) had to use a map projection to calculate the size of PIAs, which introduces distortions and errors associated with the map projection. Weiss and Overpeck (2003) considered water connectivity in their global mapping of susceptible areas, however, they did not distinguish between inundated land and inland water bodies, nor did they calculate the size of the susceptible areas.

The impacts of future sea level rise are multiple and complex considering the physical, biological, and socioeconomic aspects of the issue. The assessment of coastal vulnerability to sea level rise may be examined at several levels with increasing complexity (Klein and Nicholls, 1999). At a global scale, knowledge of the location and extent of PIAs would provide a basis from which various other impacts can be assessed. This research presents GIS-based methods to overcome the shortcomings of existing methods and to handle non-uniform cell size encountered in a global analysis. Based on the projections of sea level rise, this study assesses the global extent of potential inundation and its impact on land-cover and population within a GIS environment by addressing the following four questions:

- Where are the potentially inundated areas?
- How large are the potentially inundated areas?
- What types of land-cover, and how much of each type, are potentially inundated?
- How much of the current population would be directly impacted by potential inundation?

In addition, we provide a suite of geographic visualization products to depict both the propagation of potential inundation as well as the impact of sea level rise on the natural and built environments.

The next section discusses various sea level rise projections followed by an introduction of GIS methods developed for the analysis and describes the global datasets used in the analysis. The next sections present the results from the analysis and the various approaches for visualizing PIAs, which is followed by a discussion of the major issues encountered in the analysis and compares our results to similar studies. Finally, we present some conclusions and suggest avenues for future research.

Sea Level Rise Pr ojections

Projections of global mean sea level rise can be estimated using eustatic values computed by dividing the total water volume increase by the area of the ocean (Cooper *et al.*, 2005). During the past century, the increase in water volume is largely due to thermal expansion of the ocean, melting of mountain glaciers, and an accelerated discharge of glacial ice from the ice sheets to the ocean (Dyurgerov and Meier, 1997). Geological uplift or subsidence processes occurring in ocean basins and on continents can also influence long-term local sea level changes, and can exacerbate sea level rise impacts in many areas. All of these factors influence sea level changes on many different time scales, but the one factor that has potential for substantial global scale impacts is the melting from ice sheets.

The IPCC (2007) report acknowledges that its sea level rise appraisal does not take into account the recent rapid changes to the ice sheets that have been observed since 2003. The Greenland Ice Sheet contains a volume of water equivalent to 6 m of sea level rise, and the West Antarctic Ice Sheet, an unstable ice mass grounded well below sea level, contains a volume of water equivalent to 5 m of sea level rise (Bindschadler, 1998). Both the Greenland Ice Sheet and the West Antarctic Ice Sheet are currently showing rapid increases in mass loss that will significantly increase sea level if such mass loss continues (Thomas *et al.*, 2004; Rignot and Kanagaratam, 2006). Shepherd and Wingham (2007) have summarized the recent contributions from the Greenland and Antarctic Ice Sheets and showed a modest but growing component of the current rate of sea level rise. Otto-Bliesner *et al.* (2006) indicated that warming and melting of the Greenland Ice Sheet and other circum-Arctic ice fields likely contributed 2.2 to 3.4 meters of sea level rise during the Last Interglaciation (LIG). Overpeck *et al.* (2006) also indicated that warming polar temperature may reach a level this century similar to that of the LIG. The warmer temperature during the LIG likely contributed to ice sheet melting, which led to sea levels about four to six meters higher than present.

Mapping the areas susceptible to inundation by sea level rise is further complicated because the actual flooding process involves the level of high water, which is linked to tidal patterns and storm surges. Depending on the region, the highest water level can be several meters above mean sea level (Hoozemans *et al.*, 1993). Considering the various estimates of sea level rise reported in the literature as well as the potential effects of tidal and storm surge, we assessed the impacts of a range of sea level rise between one and six meters in this study. Although it is desirable to map the spatial variation of sea level rise, because of the lack of full understanding of the processes involved and, more importantly, the necessary data, this becomes an extremely difficult, if not impossible, task at a global scale. As a result, we estimate PIAs based on a globally uniform sea level rise. This simplification is further justifiable as we are not estimating PIAs caused by sea level rise at a certain time.

Methodologies

A series of GIS analyses were developed to address the research questions. First, PIAs were delineated based on a global DEM. Total surface area of the PIAs, surface area of

[1]Whether to remove inland water bodies is debatable, as inundation will change fresh water into sea water. We prefer to remove inland water bodies as we focus on the potential inundation of land areas but not on the study of ecological changes of fresh water bodies. In addition, not all inland water bodies are fresh water.

specific land-cover types, and population at risk within the PIAs were then calculated.

Delineating PIAs

Two methods were developed to avoid the shortcomings in previous analyses by considering water connectivity and incorporating an inland water dataset in the delineation process. Small example datasets are used to illustrate the two methods. Plate 1a shows a DEM for the example dataset and Plate 1b shows a land-cover layer with three land-cover types (ocean, inland water, and land) for the same region.

In the first method (hereafter, Method A), cells in the study area below a projected sea level rise are initially flagged (Plate 1c). From the flagged cells, only those with connectivity to the ocean are selected (Plate 1d). (Connectivity here is defined based on eight neighbors.) The selected cells are then checked to see whether or not they are part of existing inland water bodies. Only those cells that connect to the ocean and are not inland water are designated as potentially inundated cells (Plate 1e). The method is implemented as the following steps in a GIS raster analysis framework:

1. Select the DEM cells with an elevation below a projected sea level rise.
2. Identify contiguous regions from the selected cells in Step 1.
3. Create an ocean layer from the land-cover layer.
4. Combine the ocean layer with the regions identified in Step 2.
5. Select the regions that contain the current ocean.
6. Create a water layer (ocean and inland water) from the land-cover layer.
7. Subtract the water layer from the region layer in Step 5.

The second method (hereafter Method B), similar to the method developed by Weiss and Overpeck (2003), uses an iterative, custom algorithm to delineate PIAs. First, the algorithm flags all raster cells in the study area (Plate 2a) that lie adjacent to the contiguous ocean using the same eight-neighbor rule of connectivity (Plate 2b). These flagged cells represent current shoreline. Next, all cells that have an elevation value less than or equal to a projected sea level rise increment are selected (Plate 2c). Finally, all cells that are flagged in the first *and* second steps are designated as potentially inundated cells (Plate 2d). The procedure is repeated in an iterative manner until all cells of a particular elevation that are connected to the ocean are identified (Plate 2f). Plate 2e shows an interim stage of processing, part way through a complete two-meter model run using the example dataset. Once completed, existing inland water cells are subtracted from the potentially inundated cells. The method is implemented as the following steps in a GIS raster analysis framework:

1. Select DEM cells that are adjacent to ocean.
2. Select DEM cells that have an elevation at or below projected sea level rise increment.
3. Find coincidence of selected cells from Step 1 and Step 2 and convert to ocean.
4. Create potential inundation zone layer by selecting cells that were land but are now considered to be ocean.
5. Subtract existing inland water from the potential inundation zone.

Both methods delineate PIAs from a projected sea level rise based on elevation and connectivity to the current ocean, and results from the two methods are identical. Each, however, has its own advantages and disadvantages. Processing time with Method A is minimal. With the same computer configuration (Intel Pentium™ processor 1.60 GHZ with a RAM of 2 GB), a one-meter model run using Method A takes several minutes for the whole globe, whereas the same run using Method B requires several days of processing. The long processing time required for Method B is due to the multiple-stage process described above, and is a major limitation. However, because each iteration may be saved in the process, Method B allows us to display the progress of potential inundation from the existing shoreline to the extent of the entire zone after a particular increment of sea level rise is complete. Although

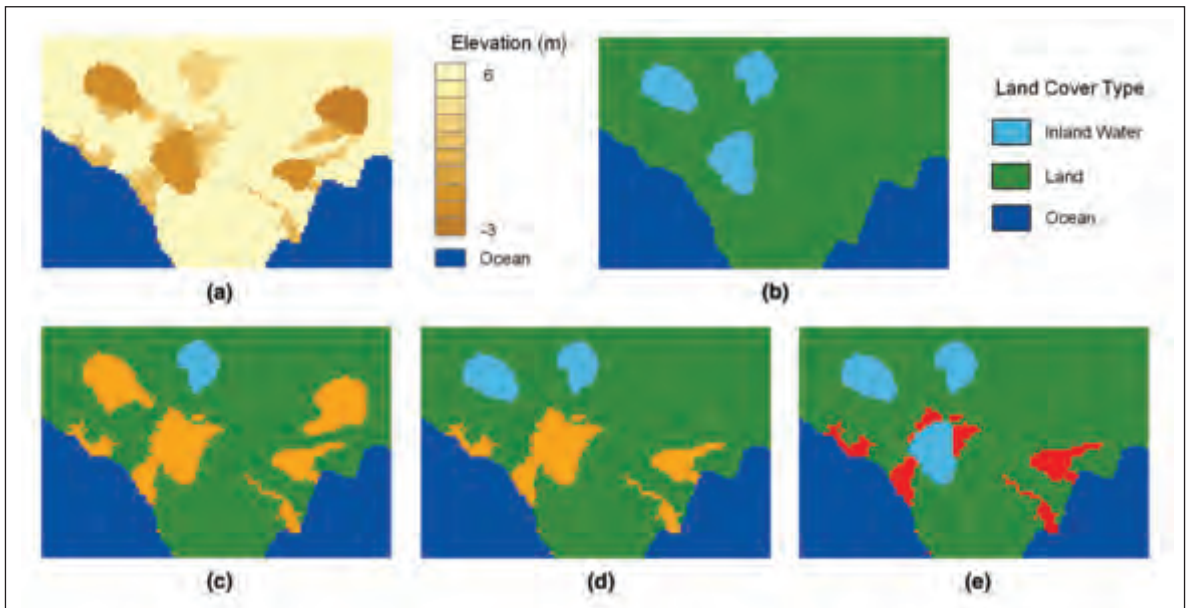

Plate 1. Small example datasets: (a) a digital elevation model, and (b) a land-cover layer, used to illustrate the GIS methods for delineating potentially inundated areas (PIA S) and the first method (Method A) for delineating PIA S; (c) areas below a projected sea level rise (orange), (d) areas below a projected sea level rise and connecting to the oceans (orange), and (e) areas inundated (red).

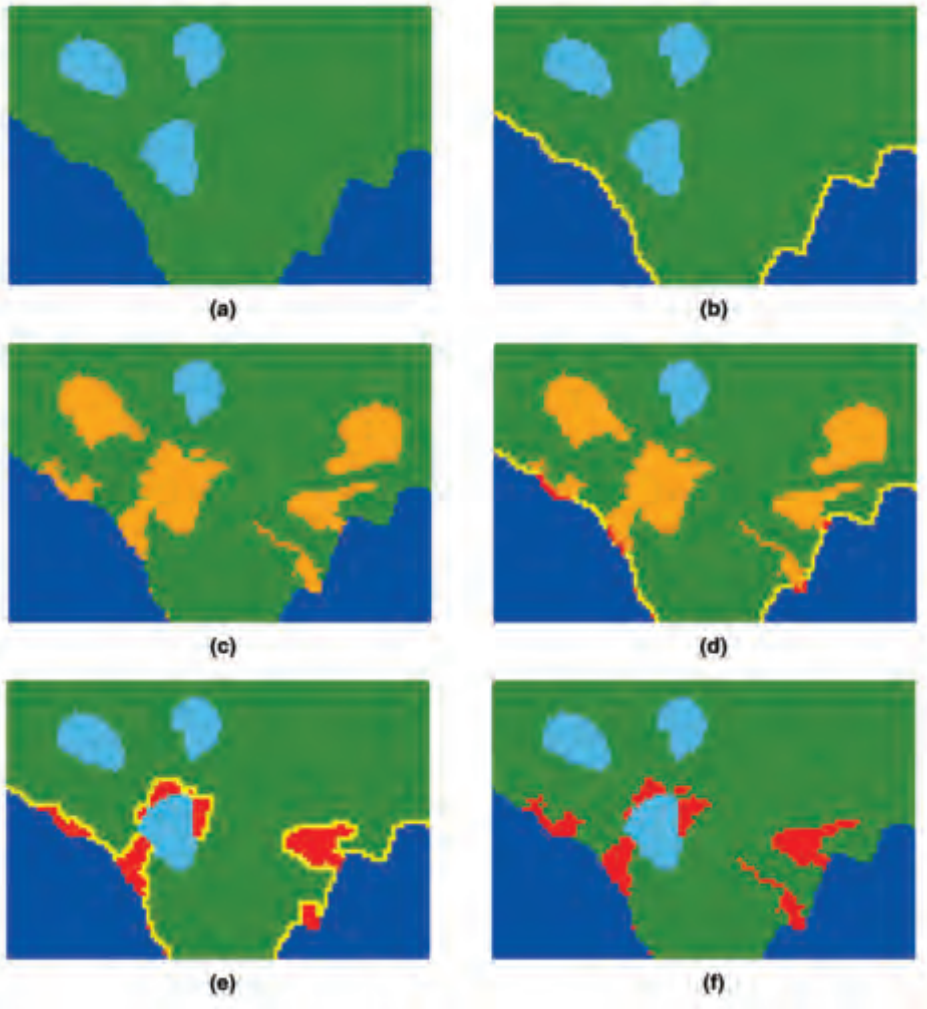

Plate 2. The second method (Method B) for delineating PIAs using the example datasets in Plate 1. The algorithm consists of multiple steps: first, areas that are adjacent to existing oceans in the original dataset (a) are selected (marked in yellow in (b)); second, areas that are below a projected sea level rise projection are selected (marked in orange in (c)); third, areas that are both adjacent to oceans and below the projected sea level rise increment are selected (marked in red in (d)); and fourth, through an iterative process propagating inland (e) until all areas within that projected increment are considered inundated (marked in red in (f)).

these intermediate passes are not estimates of sub-meter increments of sea level rise, they *simulate* the process of inundation from the shoreline to inland. Finally, the identical results from both methods not only provide a form of validation, but also allow us to use the methods for different purposes. For example, Method A is appropriate for a quick calculation of PIAs, whereas Method B is useful for demonstrating inundation progression over the landscape and is helpful for visualization efforts such as map animation.

Calculating Overall Area, the Area of each Land-cover Type, and Total Population within PIAs

The size of PIAs may be calculated easily if all raster cells have the same size. However, since the cells on a global raster layer are quadrilateral regions defined on an ellipsoidal Earth, their sizes change with bounding latitudes. Also, it is desirable to calculate the size of PIAs using the global raster layer in its original form instead of using a map projection as the projection process introduces errors and distortions. We derived the formulas for calculating the surface area of a quadrilateral region defined by the cells on the ellipsoid. Our formulas are the same as those in Bjorke and Nilsen (2004) although our derivation is different from theirs. Based on the formulas, we developed a software tool to generate a raster layer that stores the surface area at each cell. This cell-surface-area raster layer and the PIA raster layer were then used to calculate the size of PIAs through the zonal summary function in the GIS.

Surface areas of various land-cover types in the PIAs were calculated in a two-step procedure. First, the cell-surface-area layer was overlaid with the PIA layer. Next, the sub-total area of each land-cover type in the PIAs was obtained through the zonal summary function in the GIS, where the land-cover layer was the zone layer and the overlaid layer was the value layer.

Current population in the PIAs was calculated in a similar manner to land-cover using the zonal summary function in the GIS, where the PIA layer was the zonal layer and the population-per-cell layer was the value layer.

Global Datasets Used in the Analysis

Several global DEM datasets were readily available for the analysis, including the ETOPO5, ETOPO2, and GLOBE elevation datasets from the National Geophysical Data Center (NGDC) and GTOPO30 from the USGS (NGDC, 2001). ETOPO5 and ETOPO2 have horizontal resolutions of 5 minutes (approximately 10 km at the Equator) and 2 minutes (approximately 4 km at the Equator), respectively. Both the GLOBE and GTOPO30 datasets have a horizontal resolution of 30 arc-seconds (approximately 1 km at the Equator). We chose the GLOBE dataset because it is an improved version of the GTOPO30 dataset and is compiled from the best global and regional raster and vector (e.g., contours) elevation datasets available at the time of compilation (Hastings and Dunbar, 1998). In addition, the GLOBE dataset is at the same spatial resolution and datum (WGS84) as other global datasets used in the analysis (see below). Another DEM dataset derived from the Shuttle Radar Topography Mission (SRTM) has a finer spatial resolution of 90 meters. However, this dataset was not used in this study because it does not cover the entire globe (only from approximately 60° N to 60° S). In addition, it contains many artifacts that need to be rectified.

The GLOBE dataset is distributed in 16 tiles as binary files, which were first imported into the GIS as raster layers and were then merged to form a continuous global DEM dataset. PIAs were delineated using the GLOBE DEM and the methods described above with projected sea level rise from one to six meters in whole-meter increments because of the vertical resolution of the GLOBE DEM.

Population at risk within the PIAs was estimated from LandScan, a global population dataset developed by the Oak Ridge National Laboratory Global Population Project (Dobson *et al.*, 2000). LandScan was compiled from the best available population census data for each country that were then distributed into cells based on land-cover type, proximity to roads, terrain slope, and nighttime lights. LandScan has been used for a variety of humanitarian applications, such as estimating population affected by natural disasters and wartime conflicts. One major advantage of LandScan is that the spatial resolution is 30 seconds, identical to the GLOBE dataset, which allows for easy calculation of population in potentially inundated cells. The 2004 version of LandScan, the most recent version available at the time of analysis, was used.

Two global land-cover datasets are available for the analysis. Both datasets were derived from the 1992 to 1993 Advanced Very High Resolution Radiometer (AVHRR) with the same spatial resolution of 30 seconds. The first dataset was produced by the USGS for the International Geosphere-Biosphere Program (IGBP), and the second dataset was created by the University of Maryland (UMD) (Hansen and Reed, 2000). The UMD dataset provides 14 land-cover types while the USGS dataset includes 25 land-cover classes. We chose the UMD land-cover dataset for two reasons. First, we compared the consistencies in land and ocean classes (inland water bodies in the land-cover datasets were treated as land in this comparison) between both land-cover datasets and the GLOBE DEM. We found that the UMD dataset is slightly more consistent with the GLOBE dataset than the USGS dataset. Second, the UMD dataset provides more generalized land-cover types than the USGS dataset and therefore is more appropriate for global analysis.

To further simplify the land-cover classes, the original 14 land-cover types in the UMD dataset were aggregated into seven classes. For example, all the various forest classes (evergreen needle leaf, evergreen broad leaf, deciduous needle leaf, deciduous broad leaf, and mixed forests) were combined into one forest class. The seven aggregated classes were bare ground, crop land, forest, grass land, shrub land, urban and built-up, and water.

The UMD land-cover dataset served two purposes in our analysis. In addition to its use in calculating the sub-total area of each land-cover type in the PIAs, it also served as our source for building an ocean-inland water-land raster layer, which was used to remove existing water bodies in the process of delineating PIAs. In the GLOBE dataset, cells with the value of −500 are designated as ocean cells. However, we found some inland cells which are also designated as ocean, although the number of such cells is very small. We treated those cells as inland land water bodies and combined them with the inland water bodies in the UMD land-cover dataset while constructing the ocean-inland water-land raster layer.

Unlike the example datasets in Plate 1a and 1b, where shorelines in the DEM match the shorelines in the land-cover data exactly, shorelines from the GLOBE DEM, the UMD land-cover, and the LandScan datasets do not agree in all cases. For example, although 99.6 percent of the ocean cells in the GLOBE DEM are also classified as ocean in the UMD land-cover dataset, 0.1 percent and 0.3 percent of the ocean cells in the GLOBE DEM are classified as inland water and land, respectively, in the UMD land-cover dataset. Because of the inconsistency, we had to make some necessary adjustments in our calculations. For calculating the total area of PIAs and population in PIAs, we assumed that the ocean and land cells in the GLOBE dataset are correct. For calculating the area of each land-cover type in PIAs, we assumed that the ocean and land cells in the UMD dataset are correct in order to avoid counting ocean cells in the UMD dataset as PIAs in the calculation.

Analysis Results

Potential inundation at six meters in four selected regions of the world is shown in Figure 1. Notice the concentrations of potential inundation surrounding river deltas, and low-lying coastal plains. Additional maps displaying the extent of PIAs at one to six meters are available for the entire globe and for various regions at **http://www.cresis.ku.edu/research/data/sea_level_rise/index.html**. In the visualization section below, we describe additional approaches for visualizing PIAs for different increments of sea level rise. Total area of PIAs ranges from 1.055 million km^2 at the one-meter increment to 2.193 million km^2 at the six-meter increment (Table 1). The percentage of land area of PIAs for each of the sea level rise increments is also shown in Table 1.

We compared the approach of using the cell-surface-area raster layer with two simpler methods, one that assumes all the cells have the maximum cell area at the equator (i.e., 0.85 km^2) and the other that uses an average cell area. As shown in Figure 2, the maximum cell area approach greatly over-estimates the size of PIAs, which indicates that most of the potentially inundated cells are not located near the equator. Total surface area calculated using the average cell area matches quite well with our method, although the difference increases at higher sea level rise projections.

Table 2 reports the area of each land-cover type in the PIAs. As discussed in the *Global Datasets used in the Analysis* subsection, a modified version of GLOBE was used for this portion of analysis to eliminate the possibility of counting oceans in the UMD dataset as part of the PIAs. However, this change has an impact on the total area of the PIAs (i.e., the totals in Table 2 do not match with those in

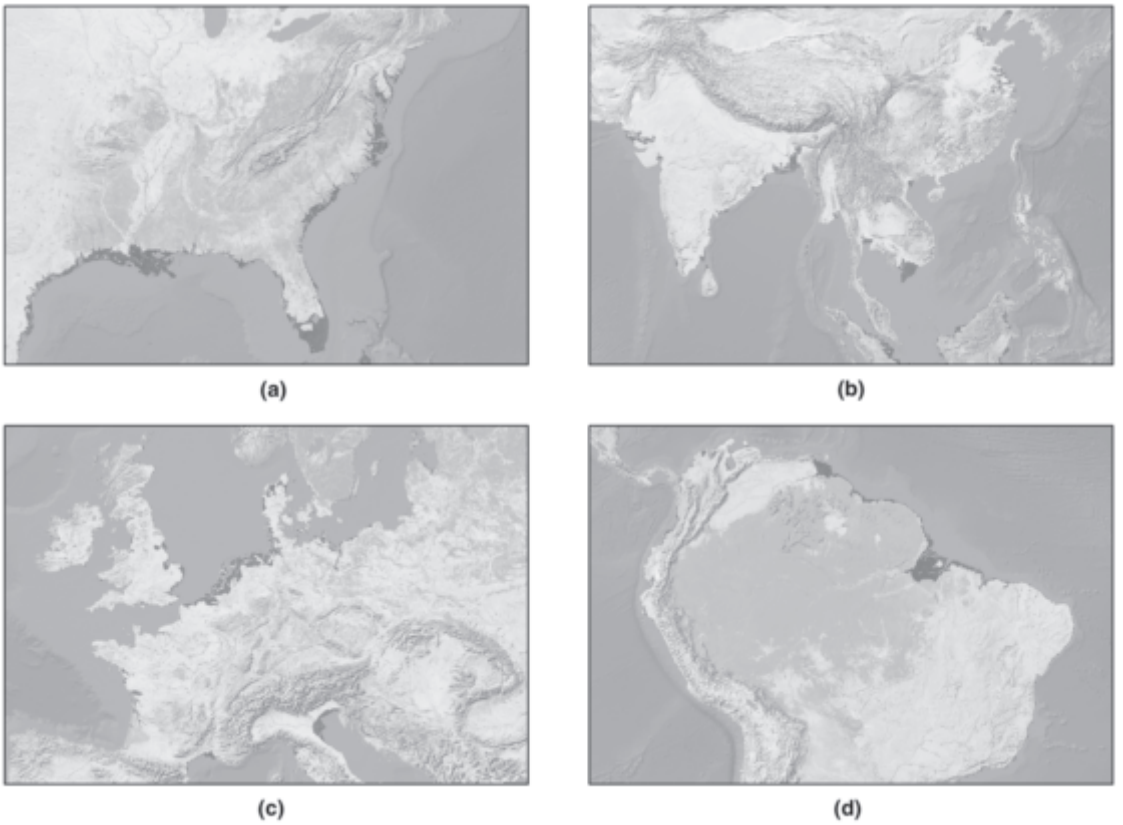

Figure 1. Selected regions of PIAs (in dark gray) resulting from a projected sea level rise of six meters: (a) Southeast USA, (b) Southeast Asia, (c) Europe, and (d) South America. Land-cover and shaded relief map are from Natural Earth (**http://www.shadedrelief.com/natural/**).

TABLE 1. TOTAL AREA OF POTENTIALLY INUNDATED AREAS (PIAS), PERCENTAGES OF LAND AREA OF PIAS, POPULATION IN PIAS, AND ITS PERCENTAGES OF TOTAL POPULATION FOR SEA LEVEL RISE FROM ONE TO SIX METERS

Sea Level Rise(m)	Inundated Area (1000 km^2)	% of Land Area	Population (millions)	% of Total Population
1	1054.99	0.7	107.94	1.7
2	1312.97	0.9	175.10	2.8
3	1538.58	1.0	233.99	3.7
4	1775.24	1.2	308.08	4.8
5	2004.37	1.4	376.26	5.9
6	2193.30	1.5	431.44	6.8

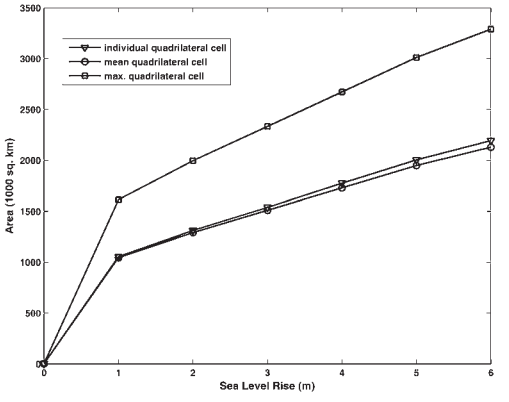

Figure 2. Total surface area of potentially inundated areas calculated using the area of each quadrilateral cell, the mean area of all quadrilateral cells, and the maximum area of all quadrilateral cells.

Table 1), with discrepancies ranging from 330,040 km^2 to 459,520 km^2 for sea level rise from one meter to six meters. Such discrepancies are an indication of the uncertainty associated with coastline delineation in the two global datasets.

Percentages of land-cover types in the PIAs for each sea level rise projection are shown in Figure 3. Among the seven land-cover types in PIAs, forest and grass land account for more than 60 percent for all the increments of sea level rise. The percentage of crop land lost increases steadily as sea level rise increases. Forest is the only land-cover type in which the percentage lost decreases with increasing sea level rise. This may suggest that a buffer zone of natural vegetation (e.g., mangrove swamps) exists at the lowest few meters above the coastline, and that crop land increases dramatically once this threshold is exceeded.

Population at risk due to potential inundation ranges from 107.9 million people at the one meter increment to 431.4 million people at the six meter increment, or nearly

TABLE 2. SUB-TOTAL AREA OF POTENTIAL INUNDATION BY SIX AGGREGATED UMD LAND-COVER TYPES

	Sub-total Area (1000 km^2)					
Land-cover	1 m	2 m	3 m	4 m	5 m	6 m
Bare ground	55.12	72.31	88.03	103.56	119.40	140.60
Crop land	41.56	71.79	104.52	134.84	173.55	200.83
Forest	256.36	311.97	357.01	401.28	445.69	482.62
Grass land	269.18	356.25	434.86	505.66	579.36	644.61
Shrub land	98.31	129.43	159.58	186.39	217.43	250.27
Urban & built-up	4.42	6.76	8.72	10.89	13.19	14.85
Total	724.95	948.51	1152.73	1342.61	1548.62	1733.78

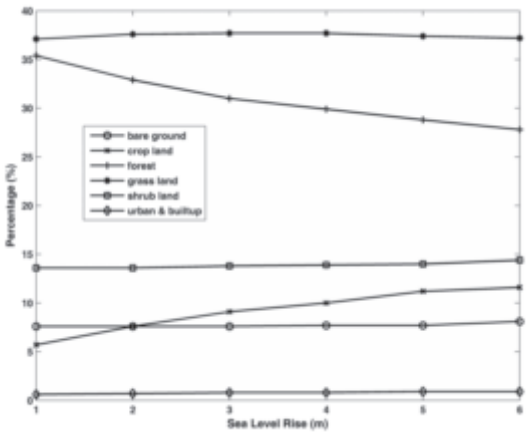

Figure 3. Percentages of sub-total area of each land-cover type in the PIAs.

2 and 7 percent of the world's population, respectively (Table 1). For all the increments of sea level rise, the percentages of population within PIAs are, by average, 3.7 times higher than the percentages of land area of PIAs. As the spatial pattern of population at risk is a major concern, in addition to our previous work (Rowley *et al.*, 2007) which computed population and land area at risk for several world regions, here we identify the top ten countries where the largest population is likely at risk for sea level rise increments from one to three meters using the country dataset provided with the LandScan dataset. Table 3 shows the lists of those countries as well as the population at risk for each increment of sea level rise. Indonesia and Vietnam are the two countries with populations most at risk to sea level rise. Another five countries (i.e., Brazil, China, India, Japan, and Netherlands) are in the lists for all the increments of sea level rise. Notice also that many of the at-risk countries are in less developed parts of the world, suggesting the potential for a catastrophic humanitarian crisis as sea level rises.

Without considering the rapid changes to the ice sheets since 2003, IPCC (2007) predicts a global mean sea level rise between 18 cm and 59 cm by 2100. A useful exercise would be to assess the potential inundation impacts of sea level rises within the range predicted by IPCC. However, due to the vertical resolution of the GLOBE DEM (i.e., whole meter increments), it is impossible to delineate PIAs at a sub-meter scale. As such, we estimated sub-meter total area and population at risk through interpolation. For surface area, we first fitted a power function of the form $y = A \cdot x^M$. Using the Gauss-Newton nonlinear least squared method, we obtained the optimal A and M, based on the second column in Table 1, as 990.05 and 0.4338, respectively. For population at risk, we fitted a similar power function to the fourth column in Table 1. The optimal A and M obtained are 99.23 and 0.8198, respectively. The power functions for total area and population are shown in Figure 4a and 4b. It should be noted, however, that the power functions were simply assumed as they are better choices than linear functions and visually fit well with the data.

As indicated in Figure 4b, the population at risk increases almost linearly with sea level rise. However, this is not the case for surface area of potential inundation, which as Figure 4a indicates, increases exponentially as sea level rise increases especially for sea level increments between zero and one meter. Using the sea level rise range predicted by the IPCC (i.e., between 18 cm and 59 cm), total

TABLE 3. TOP TEN COUNTRIES WHERE POPULATION IS LIKELY AT RISK WITH SEA LEVEL RISES FROM ONE TO THREE METERS

1 m		2 m		3 m	
Country	Population (millions)	Country	Population (millions)	Country	Population (millions)
Indonesia	17.1	Indonesia	22.1	Indonesia	26.2
Vietnam	13.4	Vietnam	19.8	Vietnam	22.9
Brazil	10.1	Japan	13.8	China	22.3
India	8.0	India	11.9	Japan	19.9
Netherlands	6.8	Brazil	11.6	India	18.0
China	6.3	Thailand	11.3	Bangladesh	17.4
Japan	4.8	China	11.2	Brazil	13.2
Australia	3.4	Bangladesh	9.9	Thailand	11.8
United Kingdom	3.4	Netherlands	7.4	Netherlands	7.9
Philippines	2.6	United States	4.3	United States	7.1

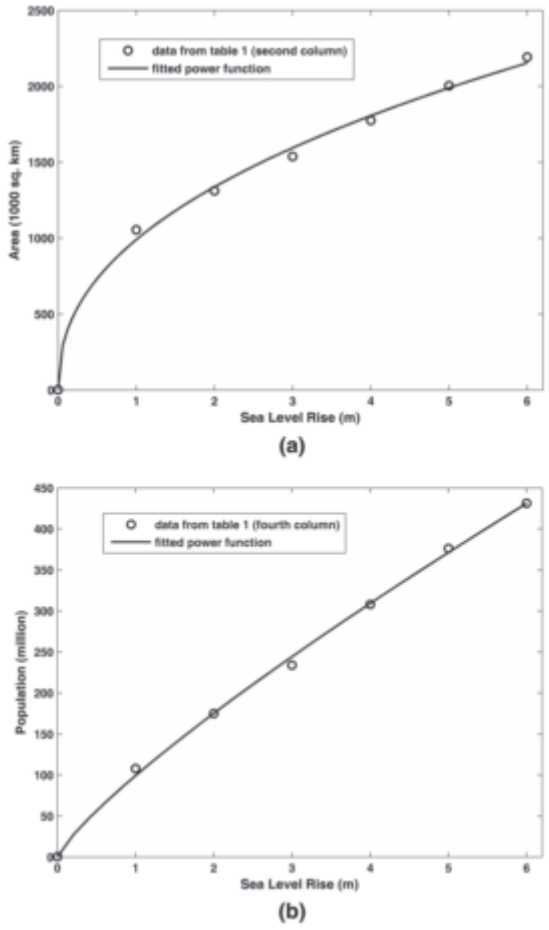

Figure 4. Power functions fitted to the data in Table 1 to interpolate (a) total surface area, and (b) population at risk in sub-meter PIAs.

surface area between 470,500 and 787,500 km^2 and population between 24.3 and 64.4 million would be at risk by 2100.

Visualizing Potential Inundation

Various methods of geographic visualization are beneficial for depicting both the propagation of potential inundation as well as the probable impact of sea level rise on the natural and built-up environments. Because different audiences may prefer different methods of data representation (Slocum *et al.*, 2003), multiple visualization techniques should be used to convey the geographic dimensions of sea level rise at global, regional, and local scales to scientists, K-12 educators, decision-makers, and the general public. We developed two key products for visualizing potential inundation caused by sea level rise: (a) map animations, and (b) layers for use in 3D GIS data viewers such as Google Earth©. Both products are freely available to the public at **http://www.cresis.ku.edu/research/data/sea_level_rise/index.html**.

To depict the possible spatial propagation of potential inundation, we developed a map animation that simulates sea level rise from zero to six meters. Animated map displays have been developed to depict the temporal and geographic aspects of numerous climate-related topics, such as mean annual temperature change for the United States from 1897 to 1986 (Weber and Buttenfield, 1993), weekly global land surface and ocean temperature patterns (Harrower *et al.*, 2000), and the depletion of ozone over Antarctica from 1979 to 1991 (Treinish, 1992). Weiss and Overpeck (2003) developed animations of sea level rise for several regions of the world. However, an important limitation of their animations is the fact that they are constructed from only one frame for each of the one to six meter increments, which does not yield a smooth transition between animation frames. In order to take fullest advantage of animation, we used Method B (discussed in the Methodologies Section) to output several iterations for each sea level rise increment as separate maps, which were then assembled as frames in standard QuickTime© animation software to create a smooth animation depicting the possible progression of inundation. Since the 30-second spatial resolution of the GLOBE DEM is too fine for viewing sea level rise projections at a global scale on computer displays, we computed PIAs from the coarser-resolution ETOPO2 dataset to fill that role. Our original computations from GLOBE, however, were used for finer-scale, regional views within the animation. The animation provides basic interactive features, such as options for users to turn on/off major cities and LandScan population underlying the PIAs, as well as the functionality for users to zoom in to various regions around the world. Due to the global variation in potential inundation, a unique frame rate was specified for each of the regional-scale animations.

Although inundation can be considered a temporal event, the map animation does not display an estimated time period (i.e., year) for each sea level rise increment (i.e., one meter). Rather, a continuous rate is indicated with a vertical bar that displays the level of potential inundation from zero to six meters. However, temporal progression is indirectly implied as the map animation progresses from zero to six meters since it would take time for water to "flow" inland over the PIAs. For some regions where large masses of land exist at a relatively low elevation (e.g., one meter), the propagation of the potentially inundated zone would occur more quickly than at a location with sharper relief. For example, map animation viewers may note the rapid inundation of the Amazon River delta at one meter, followed by a slower inward flooding along the river at two to six meters (Figure 5).

Three-dimensional GIS data viewers such as Google Earth© and ESRI's ArcGIS Explorer© are also beneficial for exploring the impact of sea level rise on the natural and built environments, particularly in urban coastal areas with large populations. An advantage of GIS data viewers such as Google Earth© and ArcGIS Explorer© is that they integrate multiple data sources (e.g., high-resolution satellite imagery, topography, etc.) in 3D displays with easy-to-use interfaces that are readily available to those with little GIS experience. For example, users may navigate in Google Earth© through a coastal city such as Miami, Florida and explore the potential impact of sea level rise on the city's infrastructure by enabling layers such as 3D buildings, roads, and satellite imagery (Plate 3).

Discussion

Compared to our methods, the simple method of delineating PIAs that does not consider water connectivity and inland water bodies over-predicts the size of PIAs from 86.4 percent (one meter) to 50.6 percent (six meters). Such large differences are caused by the Caspian Sea, which is considered a PIA by the simple method for all the sea level rise increments. Even after removing the Caspian Sea, over-prediction of the size of the PIAs still ranges from 12.4 percent (one meter) to 8.3 percent (six meters) by the simple method for the same range of sea level rise. It is noteworthy that

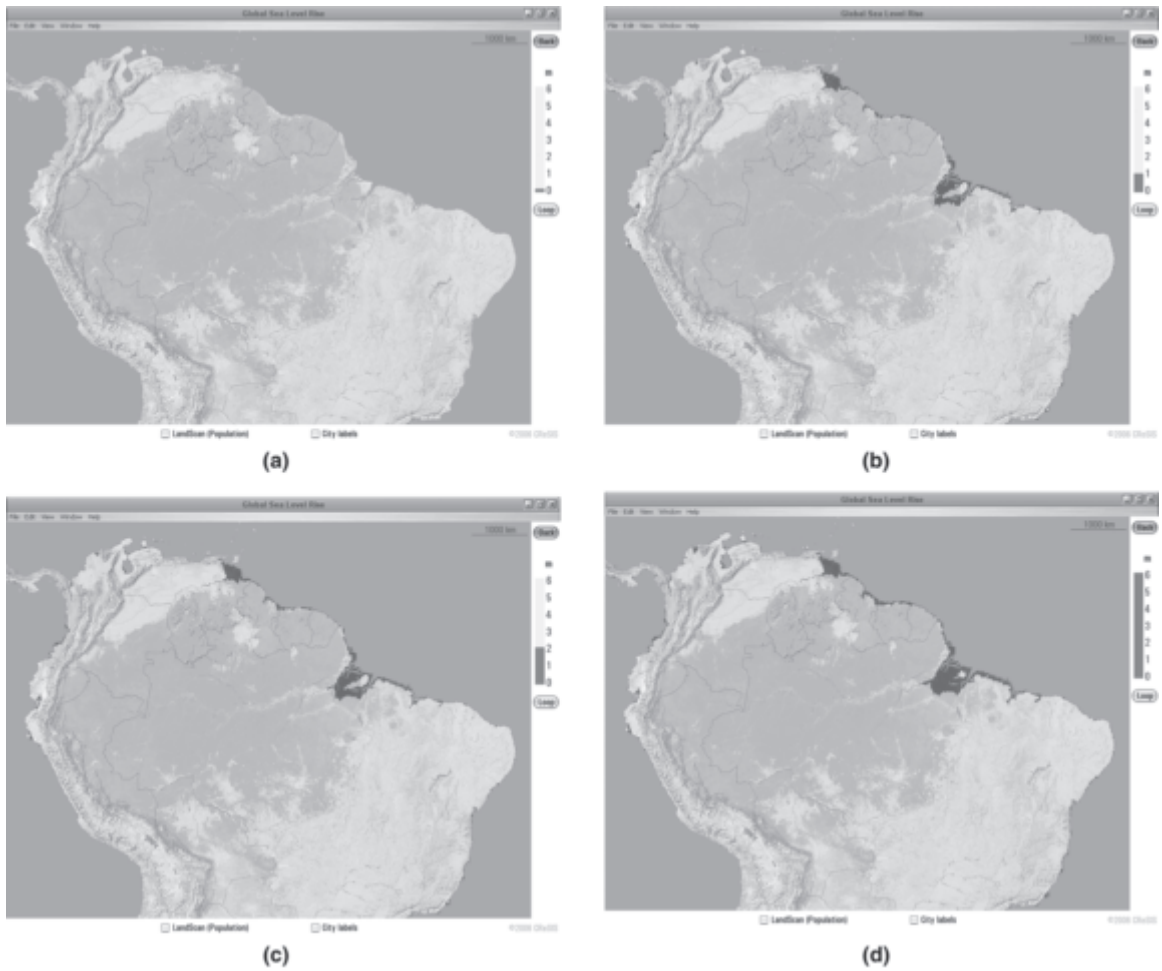

Figure 5. Screenshots from a QuickTime map animation displaying the process of inundation (in dark gray) along the Amazon River Delta in South America at (a) zero, (b) one, (c) two, and (d) six meters of sea level rise. Land-cover and shaded relief map are from Natural Earth (**http://www.shadedrelief.com/natural/**). Note that the spatial resolution of the background layers from Natural Earth is much finer than that of the GLOBE DEM.

over-prediction with low sea level rise is larger than that with high sea level rise.

Nicholls (2002) estimated that the number of people exposed to flooding by storm surges in 2100 would range between 459 to 688 million and 503 to 755 million people for 55 cm and 96 cm of sea level rise, respectively. Our estimates of population at risk at 59 cm and one meter of sea level rise are 64 and 108 million people, respectively, which is significantly less. Such a large discrepancy may lie in the fact that Nicholls (2002) considered the influence of sea level rise on storm surges and estimated the population as people living below the 1,000-year storm surge elevation. In addition, Nicholls (2002) used projected population of 2100 at the country scale, whereas our estimates are based on current population. Dasgupta *et al.* (2007) estimated that the size of impacted areas would be from 194 to 769 million km^2 and impacted population from 56 to 246 million for sea level rise from one to five meters. Compared with the numbers in Tables 1 and 3, our estimates are larger than those of Dasgupta *et al.* (2007), which are expected, as their results were based on 84 developing countries only. Although they did not provide any numbers, we visually compared our maps with those of Weiss and Overpeck (2003). The PIAs on both sets of maps looked similar but differences are visible. Such differences are largely because our method removed inland water bodies from inundation and the DEMs used in the two studies are slightly different.

The results of our analysis should be used with caution, however, due to several methodology and data limitations. First, our methods did not take into account the influence of sea level rise on high water level which is important to compute accurate flood risk maps (Anthoff *et al.*, 2006). Second, our methods did not consider the effects of existing protections, such as dikes, and future adaptations to reduce sea level rise risk (Nicholls and Tol, 2006; Tol *et al.*, 2006; McGranahan *et al.*, 2007). Third, the use of a uniform sea level rise ignores the fact that changes in sea level do not occur uniformly around the world (IPCC, 2007). Geological uplift or subsidence processes occurring in ocean basins and on continents can influence local sea level changes and regional responses could differ substantially due to the various mechanisms that cause sea level rise. Clark and Lingle (1977) and Mitrovica *et al.* (2001) have shown, for example, how the mass fluctuations of polar ice sheets could introduce the spatial variations of sea level rise. In addition, we did not analyze the economic impacts of PIAs,

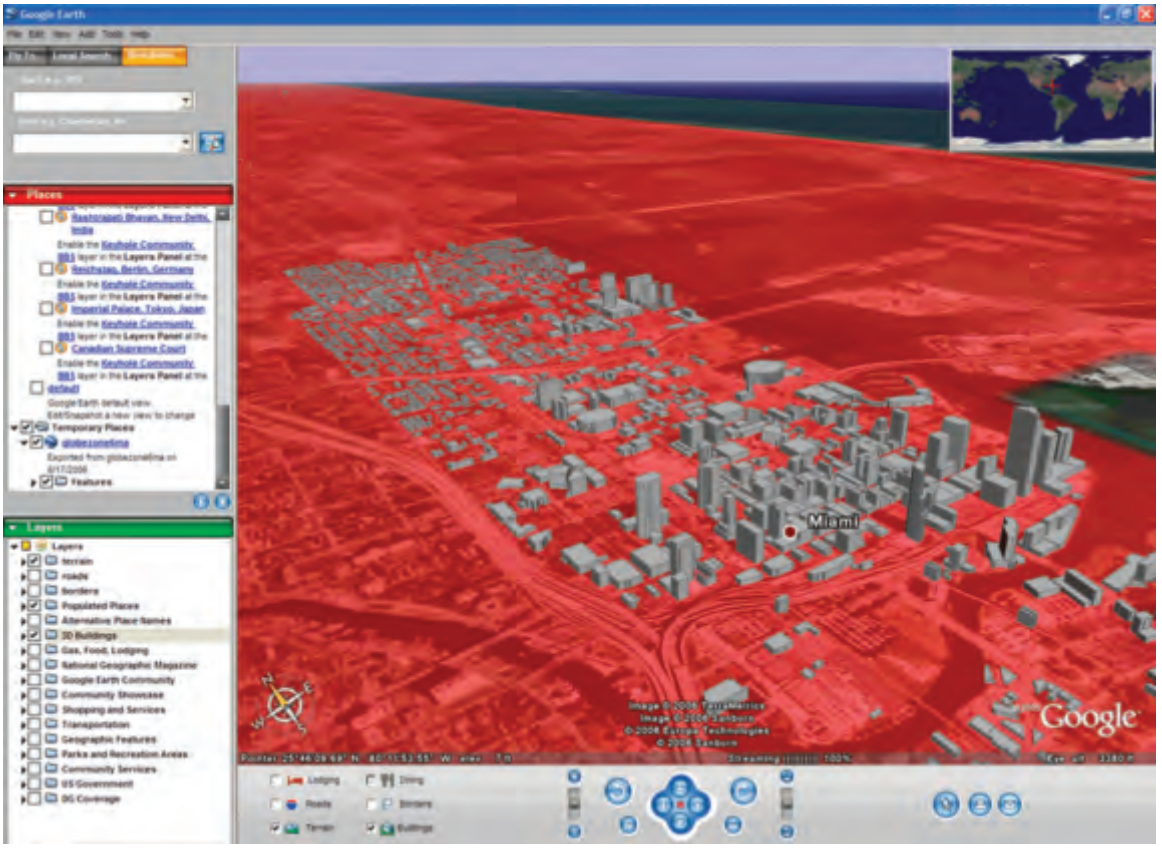

Plate 3. PIAs at six meters (in red) displayed in Google Earth © for downtown Miami, Florida with satellite imagery and 3D buildings layers enabled.

and no projections on future land-cover and population change were made in our analysis.

As for global datasets, the vertical resolution of the GLOBE dataset in whole meter increments is a limitation as it prevents direct delineation of PIAs below one meter. The GLOBE dataset also has several data quality issues. Striping and block artifacts are evident in the dataset. Cells without elevation values and land cells with negative elevation values that are adjacent to ocean cells are also found in various locations. The inconsistency of shorelines between the GLOBE, UMD, and LandScan datasets creates additional data discrepancies. Additionally, the GLOBE elevation is referenced to mean sea level, which itself changes with time. A more useful reference plane for elevation for sea level rise analysis would be an ellipsoid model of the Earth such as the WGS84 ellipsoid.

Although we provide interactive visualization methods to better display small PIAs, it is still difficult to visually search and identify contiguous regions from the potential inundation maps given that the PIAs are only a small fraction of the entire Earth's surface. For example, it may be hard to find on the map contiguous PIAs that are of a certain size and contain the largest population at risk. Exploratory data analysis and additional visualization tools still need to be developed to answer such questions.

Conclusions

This study has developed a set of GIS analysis methods to estimate the location, extent, and impacts of potential inundation resulting from different sea level rise projections at a global scale. These methods overcome several shortcomings of previous analyses. The methods were used to delineate potentially inundated areas, to calculate the total and land-cover sub-total surface area of the PIAs, and to estimate the population at risk in the PIAs. This study also proposed interactive visualization techniques to better display the progress and impacts of potential inundation on maps. The analysis was performed with the best global datasets currently available. The results from the analysis show how GIS and global datasets can be used to answer basic questions about the impacts of global climate change, though recognizing that various methodology and data limitations exist. As many of the global datasets utilized in the research were collected remotely, technological development in remote sensing will continue to benefit such global analyses.

The analyses and results are intended for use by the scientific community, but we have also added features that make them informative and understandable to the general public, K-12 students and teachers, and policy makers. Climate change, tropical storms, and tsunamis are Earth science topics that are closely followed by the public and are covered in education curricula, and this work allows the specialist and non-specialist alike to assess the impact of an inundation virtually anywhere in the world. What we do as a society to address global climate change will largely be driven by an assessment of the costs of doing nothing, and this work contributes to accurately assessing these costs.

Future work will primarily focus on improving the accuracy of determining the risks of sea level rise by

considering the influence of sea level rise on local high water level, the effects of constant and evolving protections, and the spatial variation of sea level rise caused by melting polar ice sheets. In addition, the issue of spatial and vertical resolutions of the DEM and whether the GIS methods capture the actual physical processes of inundation need to be studied further.

Acknowledgments

The authors wish to thank Nathaniel Haas and Keith French of the University of Kansas for cartographic assistance, and Asif Iqbal and Amber Reynolds of Kansas Geological Survey for serving the inundation maps on Google Earth©. We also thank Dr. Johan Feddema and Dr. Jerry Dobson of the University of Kansas as well as the three anonymous reviewers for providing insightful comments that improved the manuscript. This research was supported by the National Science Foundation under Grant Numbers 0424589, 0122520, and 0407827.

References

Anthoff, D., R.J. Nicholls, R.S.J. Tol, and A.T. Vafeidis, 2006. Global and regional exposure to large rises in sea-level: A sensitivity analysis, *Working Paper 96*, Tyndall Center for Climate Change Research, Norwich, UK.

Bindschadler, R.A., 1998. Future of the west Antarctic ice sheet, *Science*, 282:428–429.

Bjorke, J.T., and S. Nilsen, 2004. Examination of a constant-area quadrilateral grid in representation of global digital elevation models, *International Journal of Geographical Information Science*, 7:653–664.

Boruff, B.J., C. Emrich, and S.L. Cutter, 2005. Erosion hazard vulnerability of US coastal counties, *Journal of Coastal Research*, 21(5):932–942.

Clark, J.A., and C.S. Lingle, 1977. Future sea-level changes due to West Antarctic ice sheet flunctuations, *Nature*, 269:206–209.

Church, J.A., and N.J. White, 2006. A 20th century acceleration in global sea-level rise, *Geophysical Research Letters*, 33:L01602.

Cooper, M.J.P., M.D. Beavers, and M. Oppenheimer, 2005. Future sea level and the New Jersey coast, URL: *http://www.njpirg.org/NJ.asp?id2=24429&id3=NJ* (last date accessed: 26 March 2009)

Dasgupta, S., B. Laplante, C. Meisner, D. Wheeler, and J. Yan, 2007. The impact of sea level rise on developing countries: a comparative analysis, World Bank Policy Research Working Paper 4136, URL: *http://papers.ssrn.com/sol3/papers.cfm?abstract_id=962790#PaperDownload* (last date accessed: 26 March 2009)

Dobson, J.E., E.A. Bright, P.R. Coleman, R.C. Durfee, and B.A. Worley, 2000. LandScan: A global population database for estimating populations at risk, *Photogrammetric Engineering & Remote Sensing*, 66(7):849–857.

Dyurgerov, M.B., and M.F. Meier, 1997. Year-to-year fluctuations of global mass balance of small glaciers and their contribution to sea-level changes, *Arctic and Alpine Research*, 29:392–402.

Gornitz, V., S. Couch, and E.K. Hartig, 2001. Impacts of sea level rise in the New York City metropolitan area, *Global Planet Change*, 32:61–88.

Hansen, M.C., and B. Reed, 2000. A comparison of the IGBP DISCover and University of Maryland 1km global land-cover products, *International Journal of Remote Sensing*, 21:1365–1373.

Harrower, M., A.M. MacEachren, and A.L. Griffin, 2000. Developing a geographic visualization tool to support earth science learning, *Cartography and Geographic Information Science*, 27:279–293.

Hastings, D.A., and P.K. Dunbar, 1998. Development and assessment of the Global Land One-km Base Elevation Digital Elevation Model (GLOBE), *International Archives of Photogrammetry and Remote Sensing*, 32:218–221.

Hennecke, W.G., 2004. GIS-Based coastal behavior modeling and simulation of potential land and property loss: Implications of sea-level rise at Collaroy/Narrabeen beach, Sydney (Australia), *Coastal Management*, 32:449–470.

Hoozemans, F.M.J., M. Marchand, and H.A. Pennekamp, 1993. *A Global Vulnerability Assessment: Vulnerability Assessment for Population, Coastal Wetlands and Rice Production on a Global Scale*, Second edition, Delft Hydraulics, Delft, Netherlands, 180 p.

Huang, Z., Y. Zong, and W. Zhang, 2004. Coastal inundation due to sea level rise in the Pearl River delta, China, *Natural Hazards*, 33:247–264.

Intergovernmental Panel on Climate Change (IPCC), 2007. *Climate Change 2007: The Physical Science Basis - Contribution of Working Group I to the Fourth Assessment Report of the Intergovernmental Panel on Climate Change* (Solomon, S., D. Qin, M. Manning, Z. Chen, M. Marquis, K.B. Averyt, M. Tignor, and H.L. Miller, editors), Cambridge University Press, Cambridge, United Kingdom and New York, New York, 996 p.

Klein, R.J.T., and R.J. Nicholls, 1999. Assessment of coastal vulnerability to climate change, *Ambio*, 28(2):182–187.

Marbaix, P., and R.J. Nicholls, 2007. Accurately determining the risks of rising sea level, *EOS Transactions*, 88(43):441–442.

McGranahan, G., D. Balk, B. Anderson, 2007. The rising tide: Assessing the risks of climate change and human settlements in low elevation coastal zones, *Environment and Urbanization*, 19:17–37.

Mitrovica, J.X., M.E. Tamisiea, J.L. Davis, and G.A. Milne, 2001. Recent mass balance of polar ice sheets inferred from patterns of global sea-level change, *Nature*, 409:1026–1029.

National Geophysical Data Center 2001 Topography data and images, URL: *http://www.ngdc.noaa.gov/mgg/topo/topo.html* (last date accessed: 26 March 2009)

Nicholls, R.J., 2002. Analysis of global impacts of sea-level rise: A case study of flooding, *Physics and Chemistry of the Earth*, 27:1455–1466

Nicholls, R.J., 2004. Coastal flooding and wetland loss in the 21st century: Changes under the SRES climate and socio-economic scenarios, *Global Environmental Change*, 14:69–86.

Nicholls, R.J., and R.S.J. Tol, 2006. Impacts and responses to sea-level rise: A global analysis of the SRES scenarios over the twenty-first century, *Philosophical Transactions of the Royal Society A*, 364:1073–1095.

Nicholls, R.J., and C. Small, 2002. Improved estimates of coastal population exposure to hazards released, *EOS Transactions*, 83:303–305.

Nicholls, R.J., F.M.J. Hoozemans, and M. Marchand, 1999. Increasing flood risk and wetland losses due to global sea-level rise: regional and global analyses, *Global Environmental Change*, 9:S69–S87.

Otto-Bliesner, B.L., S.J. Marshall, J.T. Overpeck, G.H. Miller, and A. Hu, 2006. Simulating Arctic climate warmth and icefield retreat in the last intergalciation, *Science*, 311:1751–1753.

Overpeck, J.T., B.L. Otto-Bliesner, G.H. Miller, D.R. Muhs, R.B. Alley, and J.T. Kiehl, 2006. Paleoclimatic evidence for future ice-sheet instability and rapid sea-level rise, *Science*, 311:1747–1750.

Rahmstorf, S., 2007. A semi-empirical approach to projecting future sea-level rise, *Science*, 315:368–370.

Rignot, E, and P. Kanagaratam, 2006. Changes in the velocity structure of the Greenland Ice Sheet, *Science*, 311:986–990.

Rowley, R.J., J.C. Kostelnick, D. Braaten, X. Li, and J. Meisel, 2007. Risk of rising sea level to population and land area, *EOS Transactions*, 88:105, 107.

Shepherd, A., and D. Wingham, 2007. Recent sea-level contributions of the Antarctic and Greenland ice sheets, *Science*, 315:1529–1532.

Slocum, T.A., D. Cliburn, J.J. Feddema, and J.R. Miller, 2003. Evaluating the usability of a tool for visualizing the uncertainty of the future global water balance, *Cartography and Geography Information Science*, 30:299–317.

Thieler, E.R., J. Williams, and E. Hammer-Klose, 2000. National assessment of coastal vulnerability to sea level rise, URL: *http://woodshole.er.usgs.gov/project-pages/cvi/* (last date accessed: 26 March 2009).

Thomas, R., E. Rignot, G. Casassa, P. Kanagaratnam, C. Acuña, T. Akins, H. Brecher, E. Frederick, P. Gogineni, W. Krabill,

S. Manizade, H. Ramamoorthy, A. Rivera, R. Russell, J. Sonntag, R. Swift, J. Yungel, J. Zwally, 2004. Accelerated sea-level rise from West Antarctica, *Science*, 306:255–258.

Titus, J.G., R.A. Park, S.P. Leatherman, J.R. Weggel, M.S. Greene, P.W. Mausel, S. Brown, G. Gaunt, M. Treha, and G. Yohe, 1991. The cost of holding back the sea, *Coastal Management*, 19:171–204.

Titus, J.G., and C. Richman, 2001. Maps of lands vulnerable to sea level rise: modeled elevation along the US Atlantic and Gulf coasts, *Climate Research*, 18:205–228.

Tol, R.S.J., M. Bohnd, T.E. Downinge, M.-L. Guillerminetf, E. Hizsnyikg, R. Kaspersond, K. Lonsdalee, C. Maysh, R.J. Nicholllsi, A.A. Olsthoornb, G. Pfeifleh, M. Poumadereh, F.L. Tothg, N. Vafeidisk, P.E. van der Werffb, and I.H. Yetkinerl, 2006. Adaptation to five meters of sea level rise, *Journal of Risk Research*, 9:467–482.

Treinish, L.A., 1992. *Climatology of Global Stratospheric Ozone*, Videotape, IBM Corporation.

Weber, C.R., and B.P. Buttenfield, 1993. A cartographic animation of average yearly surface temperatures for the 48 contiguous United States: 1897–1986, *Cartography and Geographic Information Systems*, 20:141–150.

Weiss, J.L., and J.T. Overpeck, 2003. Climate change and sea level, URL: *http://www.geo.arizona.edu/dgesl/research/other/climate_change_and_sea_level/sea_level_rise/sea_level_rise.htm*, University of Arizona (last date accessed: 26 March 2009).

Wu, S.Y., B. Yarnal, and A. Fisher, 2002. Vulnerability of coastal communities to sea-level rise: a case study of Cape May County, New Jersey, USA, *Climate Research*, 22:255–270.

Zhang, K., B.C. Douglas, and S.P. Latherman, 2004. Global warming and coastal erosion, *Climatic Change*, 64:41–58.